Structural Engineering International

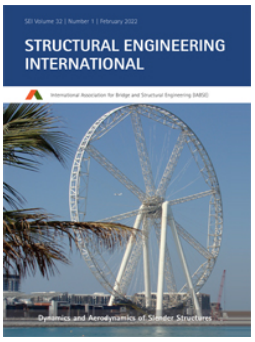

ISSN: (Print) (Online) Journal homepage: https://www.tandfonline.com/loi/tsei20

Graphical Stability Analysis of Maillart's Roof at Chiasso

Allan McRobie Prof., Cameron Millar MEng Student, Denis Zastavni Prof. & William Baker Prof.

Graphical Stability Analysis of Maillart's Roof at Chiasso

Allan McRobie, Prof.; **Cameron Millar,** MEng Student, Department of Engineering, University of Cambridge, Cambridge, UK; **Denis Zastavni,** Prof., Faculty of Architecture, Architectural Engineering and Urbanism, Université Catholique de Louvain, Louvain-la-Neuve, Belgium; **William Baker,** Prof., Skidmore Owings & Merrill, Chicago, IL, USA. Contact: fam20@cam.ac.uk

DOI: 10.1080/10168664.2021.2018958

Abstract

The newly-developed method of *graphic stability* is applied to Robert Maillart's iconic roof design at Chiasso. The truss has an unusual form that emerged from Maillart's graphic statics as the shape dual to the symmetrical equilibrium forces. Although graphic statics can lead to highly efficient structural forms, there can be a tendency for diagonal bracing to be minimised or even eliminated, as at Chiasso. Whilst equilibrium is satisfied, there may be a decrease in stability, and it has not previously been possible to quantify this within the traditional graphical approach. Using Chiasso as an example, this paper demonstrates how the prestress stability of this and similar truss structures may now be assessed within the same graphical setting.

Keywords: Chiasso; roof; truss; stability; Maillart; graphic statics

Introduction

In this paper, the methods of graphical stability analysis recently developed in Ref. [1] are applied to Robert Maillart's famous 1925 truss design for the Magazzini Generali shed roof at Chiasso, Switzerland (*Fig. 1*). In this iconic design, Maillart used graphic statics to guarantee equilibrium, and the shape of the truss emerged as the form that most naturally provides equilibrium.[2,3] The dominant loads are symmetrical and are carried by the collaboration of purely axial bar forces in the funicular tension members below and the kinked compression chord of the roof above. This paper goes beyond equilibrium to stability.

With origins that date back to Stevin[4] in 1586 and Varignon[5] in 1687, graphic statics is a way of determining the equilibrium forces in structures by purely graphical means. Typically, these are two-dimensional pin-jointed trusses, although there are methods that deal with arches and beams, and there have even been attempts to analyse 3D structures. Considerable advances were made in the late nineteenth century by Maxwell,[6,7] Cremona,[8] Culmann[9] and others. Maillart learned the techniques from Wilhelm Ritter whilst a student at ETH in Zurich in the 1890s, Ritter having been the main assistant and successor of Culmann. Although most modern structural analyses now employ computerised matrix methods, there has been renewed interest in graphic statics, and particularly in the way that it can be used to arrive at efficient structural forms. When applied to the design of trusses, however, the method can have a tendency to minimise or even eliminate diagonal bracing members, particularly if the form is optimised.[10] Such a geometrical optimum without bracing can be reached only for one reference loading case, a scenario that never occurs in actual structures. The diagonals or other forms of bracing are required for other loading cases and for stability.

It is often stated that the funicular forms that arise via graphic statics gain their efficiency by the avoidance of bending, but even standard triangulated structures such as Pratt or Warren trusses carry the applied loads via predominantly axial actions. However, optimising a triangulated morphology for a unique reference loading case leads to funicular chords and to diagonal bracing being discarded, creating the appearance of Vierendeel-like structures that nevertheless behave according to a totally different structural principle.

Given that graphic statics can lead to forms that are potentially unstable, the extension in Ref. [1] to assess the structural stability within the same graphical ansatz is an interesting development. The approach is essentially a distillation and then a graphical interpretation of Guest's matrix description[11] of the prestress stiffness of trusses.

The modern resurgence of graphic statics has been greatly bolstered by computer implementations, and its use as a design tool can lead to a rich set of economical shapes that necessarily satisfy equilibrium for the load cases considered. However, equilibrium is not enough. Stability is required, and now stability can be studied graphically. This paper illustrates the procedures, with two aims. The first is minor: it seeks to improve the understanding of Maillart's classic design. The more substantial aim is to demonstrate how the new methods can provide more general understandings of structural stability, such that these may be of use in future designs.

Background

Robert Maillart (1872–1940) stands amongst the greatest of all structural engineers. A famous early exponent of structural reinforced concrete, his bridge designs at Salginatobel (1929) and Schwandbach (1933) in Switzerland are exemplars of efficient design and aesthetic form.[12] They remain hugely influential, the Infante Dom Henrique Bridge in Porto being a recent example[13] that acknowledges Maillart's innovations.

Maillart designed the Chiasso roof around 1925. Vierendeel had proposed simplified methods for analysing his structures from the early 1900s, but Hardy Cross did not publish his method of moment distribution until

Fig. 1: Chiasso Shed (ETH-Bibliothek Zürich, image archive/Robert Maillart archive)

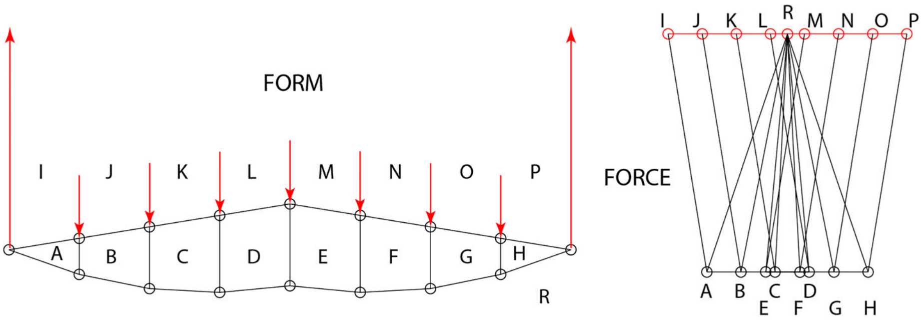

Fig. 2: A first approximation to the form and force diagrams of the central section (after Refs. [2, 3]). The Maxwell convention is used, such that corresponding bars and forces are drawn perpendicular

1930. There were thus limited tools available for analysing a rigid quad frame. However, Maillart did not envisage the roof as such a structure, and took a completely different perspective on its structural action. As explained in Refs [2,3], a graphic analysis of the roof under uniform symmetric loads leads naturally to the characteristic funicular shape of the lower chord tension members at Chiasso. *Figure 2* shows the first approximation to the reciprocal form and force diagrams for the central section of the roof.

The topology of the form diagram is first sketched and labelled, although the precise geometry of the lower chord is as yet unknown. This will be determined by constructing the force diagram. In order to match the later use of Airy stress functions better, the construction here follows Maxwell's convention, drawing bar forces perpendicular to their corresponding bars. The construction of the force diagram begins by placing nodes I, J, …, P at equal spaces along the upper horizontal, the spaces representing the applied equal loads. If the end reactions are assumed to be vertical, then node R must lie at the midpoint of line IP. Compressive forces in the roof are given by lines IA, JB, …, PH, which extend from points I, J, …, P perpendicular to the roof slope. Since the applied roof loads are collinear with the vertical members below the roof, the roof compressions are necessarily of equal magnitude across each roof node, and thus the points A–H define some lower horizontal. These points connect in turn to the central pole R, with the lines AR, BR, …, HR defining the slopes of the lower chord members and the forces therein. In this manner, the characteristic shape emerges naturally from the need for force equilibrium. It is a somewhat unusual shape, but it guarantees equilibrium for this load case. This example illustrates the power of graphic statics when used in a design setting: it would be difficult to arrive at this shape using standard matrix structural analysis tools, which generally assume that the shape is known.

It was not essential to place node R on line IP. Placing it there makes lines IR and RP horizontal, and thus the end reactions are vertical. In subsequent force diagrams, node R will be placed off the IP axis to match the actual geometry at Chiasso better.

The graphic statics explanation considers only symmetric loads. To understand the behaviour under asymmetric loads, it is worth recalling how Maillart approached this issue in his bridge designs. Rather than the more famous Salginatobel Bridge with its thickened arch, it is the deck-stiffened arches at Valtschielbach (1926), Traubach (1932), Bolbach (1932) and Schwandbach (1933) that are significant here. Maillart's first such bridge was a 41 m span over the Flienglibach in Wägital, Switzerland, designed and constructed in 1923 only a year before Chiasso.[12] The arch members for these bridges—as for the later Infante Dom Henrique in Porto—are markedly slender and unable to carry significant bending moments. In his 1949 biography of Maillart, Bill[14] goes so far as to describe the arch at Valtschielbach as "obviously too weak". The deck above, however, is deliberately thicker and capable of sustaining sizeable moments by virtue of stiff and well-reinforced parapets that run the length of the bridge. It is the combination of arch action in the slender arch below and the deck-dominated bending action of the combined system that is key to the bridge behaviour.

Following Ref. [15], *Fig. 3* shows how the combination of slender arch and stiff deck can carry the asymmetric loads. The live load is broken into symmetric and antisymmetric components, and the symmetric component can be carried efficiently via the funicular action of the symmetric arch, together with the dead loads. The remaining antisymmetric component of the live load is carried by bending action. This is shared between the deck and arch in direct proportion to their flexural rigidities. Being much stiffer, the deck will carry almost all of this. The antisymmetry enforces an effective hinge at midspan such that the deck needs to be designed for a moment of only $(w_{LL}/2)(L/2)^2/8 = w_{LL}L^2/64$, where w_{LL} is the unbalanced distributed load over half the bridge, and L is the total span. This rather startling factor of 1/64 can be found in Maillart's original calculations.[12] Maillart has thus envisaged an equilibrium system and has designed accordingly, an approach that presages the lower bound theorem of plastic design by a number of decades.

A similar analysis may be applied to the Chiasso roof. If it were a pin-jointed truss, it would be likely to undergo large deformations under any asymmetric loading. However, the roof chord and the adjacent parts of the roof slab act to form a rafter-like T-beam.[2,3] This can act in a manner similar to the stiff deck at

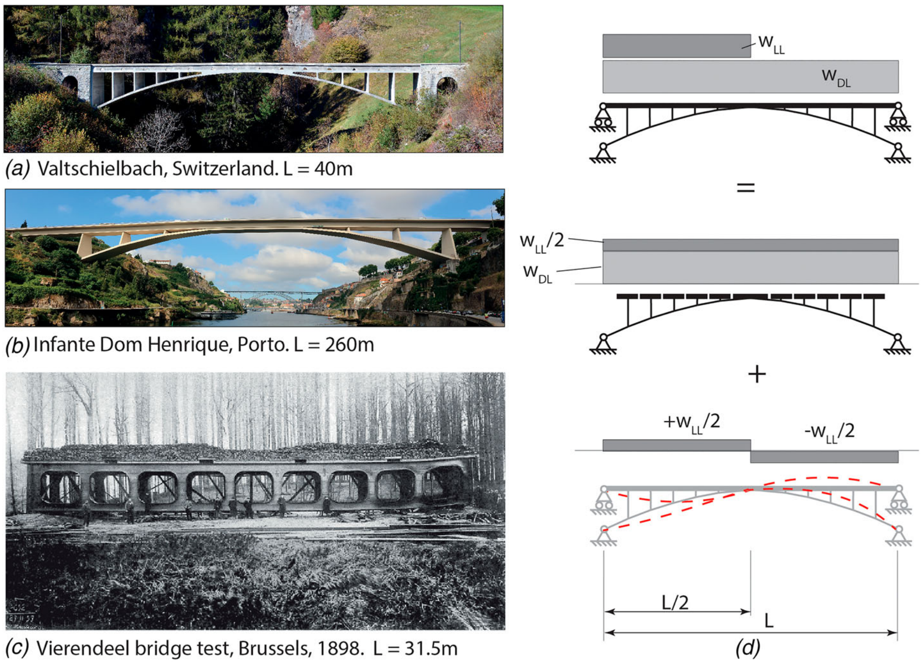

Fig. 3: (a) Valtschielbach Bridge, Switzerland, by Maillart, 1926, (b) the Infante Dom Henrique Bridge, Porto, Portugal by Adão da Fonseca, 2003, (c) bridge test in Tervuren Park, Brussels,[17] by Arthur Vierendeel, 1898, (d) decomposition of live load on deck-stiffened arch into symmetric and anti-symmetric parts (Credits: (a),(b) Adobe Stock 176664711, 446983514, (c) Lambin and Christophe, 1898).

Valtschielbach, transferring loads to the underlying funicular such that asymmetric loads can be carried by the combined system. The rigidity of the remaining joints adds further stability. The flexural rigidity of the roof T-beam may not be quite so dominant over those of the underlying members as is the case with the deck-stiffened bridges, and so there may be some limited load sharing involving bending of both upper and lower members.

Given the abundance of quads in the truss topology and the evident need for joint fixity to sustain asymmetric loading, it is tempting to compare the Chiasso truss to the forms developed by Arthur Vierendeel in Belgium around the end of the nineteenth century. It is tempting to describe any truss with diagonal-free quads as a "Vierendeel" truss. However, a Vierendeel truss needs joint fixity to carry *any* load. The need for large local bending capacity can lead to a need for very stocky members (see *Fig. 3c*).[16-18] This is not an efficient way to carry loads, but Vierendeel—Professor of Construction, Material Strength and Structural Engineering at UC Louvain—had arguments that the aesthetics of these new materials of iron and steel demanded such visual expressions of strength.[16] In comparison, the Maillart trusses—despite the quads—can carry a large portion of their loads by axial funicular action and are thus considerably leaner designs.

Against this historical background, the stability of pin-jointed trusses having geometries similar to that at Chiasso are now considered in order to demonstrate how much can be learned using the new method of "graphic stability".

Graphic Statics and Graphic Stability

Ref. [1] shows show how the stability of a pin-jointed truss with axially-rigid bars can be determined by the eigenstructure of a stiffness matrix that includes the tension–stiffening or compression–destiffening effects of the axial forces within the members. This is a major advance over traditional graphic statics, which concerns itself only with equilibrium.

Textbooks expounding how to apply the classical graphic statics of the early pioneers[4-9] to practical engineering design were provided in 1921,[19] and more recently in 2009.[20] In its simplest manifestation, the force diagram for a loaded truss is the assembly of all nodal force polygons into a single diagram. More recent expositions[21,22] have emphasised Maxwell's use of the Airy stress function[6,7] to create dual polyhedra whose 2D projections are the form and force diagrams, and the so-called Maxwell–Minkowski diagrams,[23,24] which are unified diagrams connecting the form and force polygons with rectangles of dimensions tension by length. Both will be of use in this paper, as will the extensions from statics to kinematics in Refs. [25,22] that showed how structural mechanisms can be identified graphically by considering independent increments of the Airy stress function over the force diagram. Any such increment generates a parallel motion of the form diagram, and a 90° rotation of the incremental nodal displacements gives an infinitesimal mechanism. As per usual, an independent set of such mechanisms spans the null space of the structure's compatibility matrix. Indeed, the alternative (non-graphical) way to obtain a basis set of mechanisms is simply to form the compatibility matrix and extract its null space.

The novelty introduced in Ref. [1] is the method for equipping this set of mechanisms with the effects of prestress, and thereby quantifying the extent to which bar tensions and compressions will tend to stabilise and destabilise. The effects of external loads are incorporated within the bar summation and need not be included separately. Following Ref. [1] let the structure be in an equilibrium state of self-stress with bar tensions $\{T_i\}$ and lengths $\{L_i\}$. Let each bar i rotate by θ_i as the structure moves in the infinitesimal mechanism M about the equilibrium configuration. The total potential energy Π associated with the motion is then

$$\Pi(M) = \frac{1}{2}\sum\nolimits_{\text{bars}} T_i L_i \theta_i^2 \qquad (1)$$

If this quantity is positive, then the axial forces stabilise the mechanism M. If the quantity is negative, the mechanism is unstable for that load case. Further details are provided in Ref. [26].

The form and force information of the underlying equilibrium state can be combined into a single geometrical object[23,24] called the Maxwell–Minkowski diagram. In such a diagram, the structural bars are replaced by rectangles with edge dimensions of bar force T and bar length L. The total potential energy of any mechanism is thus the weighted sum of these rectangular areas, the weights being half the square of the bar rotations caused by the mechanism. Loosely speaking, for a mechanism to be stable it must require the tension members to rotate more than the compression members.

The roof truss, however, possesses numerous mechanisms. A complete independent basis set of mechanisms can readily be found via the rotated incremental Airy approach, and the total potential energy—and hence the stability—of each of these can readily be checked. However, even if all basis mechanisms reveal positive stability, there may still be linear combinations that are unstable. To resolve this, the eigenstructure of the total potential energy needs to be examined. Unfortunately there is as yet no graphical construction for this step, meaning that matrices are required. Even so, the matrix formulation of Ref. [1] is novel.

The bar rotations $\boldsymbol{\theta}$ of a general mechanism may be written as a linear combination of the bar rotations $\boldsymbol{\Theta}$ of any complete set of independent basis mechanisms, such that $\boldsymbol{\theta} = \boldsymbol{\Theta}\mathbf{a}$ for some coefficient vector $\mathbf{a}$. This leads to a quadratic form for the energy:

$$\Pi = \frac{1}{2}\,\mathbf{a}^{\mathrm{T}}\boldsymbol{\Theta}^{\mathrm{T}}\,(TL)\,\boldsymbol{\Theta}\mathbf{a} = \frac{1}{2}\mathbf{a}^{\mathrm{T}}K\,\mathbf{a} \tag{2}$$

with the prestress stiffness matrix $\mathbf{K}$ representing the stiffness supplied to the mechanisms by the bar tensions.

Let $\mathbf{W}$ be the matrix whose columns are the nodal displacements of each basis mechanism, such that a general mechanism has nodal displacements $\mathbf{w} = \mathbf{W}\mathbf{a}$, with coefficient vector $\mathbf{a}$. These motions may be readily normalised such that $\mathbf{w}^{\mathrm{T}}\mathbf{w} = 1$ for each basis mechanism individually. It need not be true that $\mathbf{u}^{\mathrm{T}}\mathbf{w} = 0$ for nodal displacements $\mathbf{u}$ and $\mathbf{w}$ arising from different mechanisms. That is, basis vectors are normalised but not necessarily orthogonal. Let any general deformation with displacements $\mathbf{w} = \mathbf{W}\mathbf{a}$ and corresponding bar rotations $\boldsymbol{\theta} = \boldsymbol{\Theta}\mathbf{a}$ define a one-dimensional family of deformations with displacements $\alpha\mathbf{w}$ and bar rotations $\alpha\boldsymbol{\theta}$. The total potential energy is then $k\alpha^2/2$ with $k = \mathbf{a}^{\mathrm{T}}\boldsymbol{\Theta}^{\mathrm{T}}$ $\mathbf{TL}$ $\boldsymbol{\Theta}\mathbf{a}$. It is now sought to vary the coefficients $\mathbf{a}$ to find the extremal values of the stiffness k, subject to the normalisation constraint that $\mathbf{w}^{\mathrm{T}}\mathbf{w} = \mathbf{a}^{\mathrm{T}}\mathbf{W}^{\mathrm{T}}\mathbf{W}\mathbf{a} = 1$. That is, a constrained optimisation problem is solved for the values of $\mathbf{a}$ that extremise the function

$$\Pi*(\mathbf{a}) = \frac{1}{2}\mathbf{a}^{\mathrm{T}}\mathbf{K}\mathbf{a} + \frac{1}{2}\lambda(1 - \mathbf{a}^{\mathrm{T}}\mathbf{W}^{\mathrm{T}}\mathbf{W}\mathbf{a}) \tag{3}$$

where $\mathbf{K} = \boldsymbol{\Theta}^{\mathrm{T}}$ $\mathbf{TL}$ $\boldsymbol{\Theta}$ and λ is a Lagrange multiplier. Stationarity leads to the generalised eigenvalue problem

$$(\mathbf{K}{-}\lambda\mathbf{B})\phi = 0 \tag{4}$$

where the matrix $\mathbf{B} = \mathbf{W}^{\mathrm{T}}\mathbf{W}$ arises due to the lack of orthogonality of the original basis. Each eigenvector $\mathbf{a} = \boldsymbol{\phi}$ corresponds to a mechanism of the unstressed system that has nodal displacements $\mathbf{w} = \mathbf{W}\boldsymbol{\phi}$ and bar rotations $\boldsymbol{\theta} = \boldsymbol{\Theta}\boldsymbol{\phi}$. Each eigenvalue λ represents the degree to which the corresponding eigen-mechanism has been stiffened or destiffened by the bar tensions and compressions, just as a pendulum is a mechanism that gains stiffness by virtue of the tensile force it carries. As usual, stability requires all eigen-stiffnesses to be positive.

To apply this analysis to the Chiasso shed, the structure is simplified. It is approximated as a 2D pin-jointed truss, with the pin joints connected by axially-rigid bars. Internal bays have span L and the end bay has span $2L$. Loads of magnitude F are applied atop each vertical hanger, except that the outermost four roof nodes each support loads of $1.5F$ in proportion to the roof lengths they support. This idealised geometry is shown in Fig. 4.

The Central Section

The focus is first on the eight-bay central section. Here, the geometry and forces are completely determined by the angles α, β and γ.[27] There are six four-bar linkages in the central section, but the end nodes must satisfy the no-displacement boundary conditions. Given so many quads and given that the loads are applied from above, the first impression may be that this section should be unstable in-plane, with the four-bar linkages free to deform in numerous ways. With no added funicular, the Maxwell count (as extended by Calladine[28]) has

$$2v - e - r = m - s$$

where there are $v = 16$ nodes, $e = 23$ bars and $r = 4$ reactions for pinned supports without rollers. There are $s = 0$ states of self-stress, and thus $m = 5$ mechanisms.

A basis set of mechanisms can readily be determined numerically by computing the nullspace of the compatibility matrix. However, in keeping with the spirit of the paper, the more graphical approach of McRobie et al.[22] is employed here. First, a funicular is added above the form diagram (see Fig. 5). Not only does this provide a means for applying the roof loads that will be needed in the stability analysis later, but it also creates a richer topology such that meaningful Airy stress functions can be defined. Note that the extra vertices and edges of the funicular add $2v - e = 2(9) - 18 = 0$, thus the Calladine sum is unchanged, giving $m - s = 5$ still. However, since the funicular geometry has been chosen such that it can create a state of self-stress for the roof loads, then there is also a sixth mechanism that involves only the funicular members, although this is of no immediate interest.

A complete set of independent mechanisms $\mathbf{M}$ is readily found by the incremental Airy approach, as illustrated in Figs. 6, 7, 8. To respect the no-

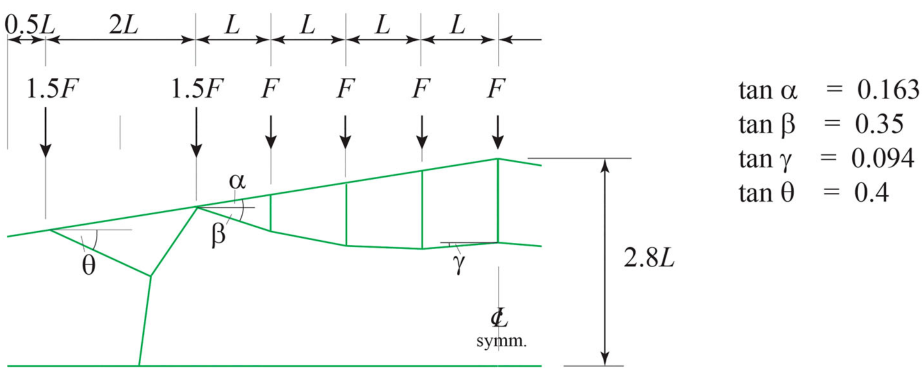

Fig. 4: Idealised geometry of the roof truss

displacement boundary conditions at the outermost nodes, all Airy stress functions over the force diagram are zero over the faces AIR and RPH (shaded in *Fig. 5*) which are reciprocal to the support nodes. Clearly, raising edge JB as a ridge whilst keeping edges IA and KC at zero maintains planarity of the adjoining quad faces. The resulting local stress function, Airy 1, is shown in *Fig. 6*.

There are four independent stress functions of this general form, involving ridges JB, KC, NF and OG in turn. For the fifth, the crossed-quad face LMED can be raised uniformly (see *Fig. 7*), and for the sixth, the node Q can be raised to generate the motion associated purely with the external funicular. These six incremental Airy stress functions involve motions of all the non-support nodes and form a complete basis for the mechanism analysis. Dual to each incremental stress function over the force diagram is an incremental form diagram defining a set of nodal displacements. When applied to the nodes of the original form diagram, these displacements create a parallel motion with all bars remaining parallel to their original directions. A 90° rotation of these nodal displacements then gives an inextensible mechanism of the form diagram. The procedure is illustrated in *Fig. 7* for the stress function local to the crossed-quad LMED.

The analysis thus far has been purely first order, of equilibrium and kinematics. The second order analysis of Ref. [1] is now added to equip the space of mechanisms with the stiffnesses associated with the internal

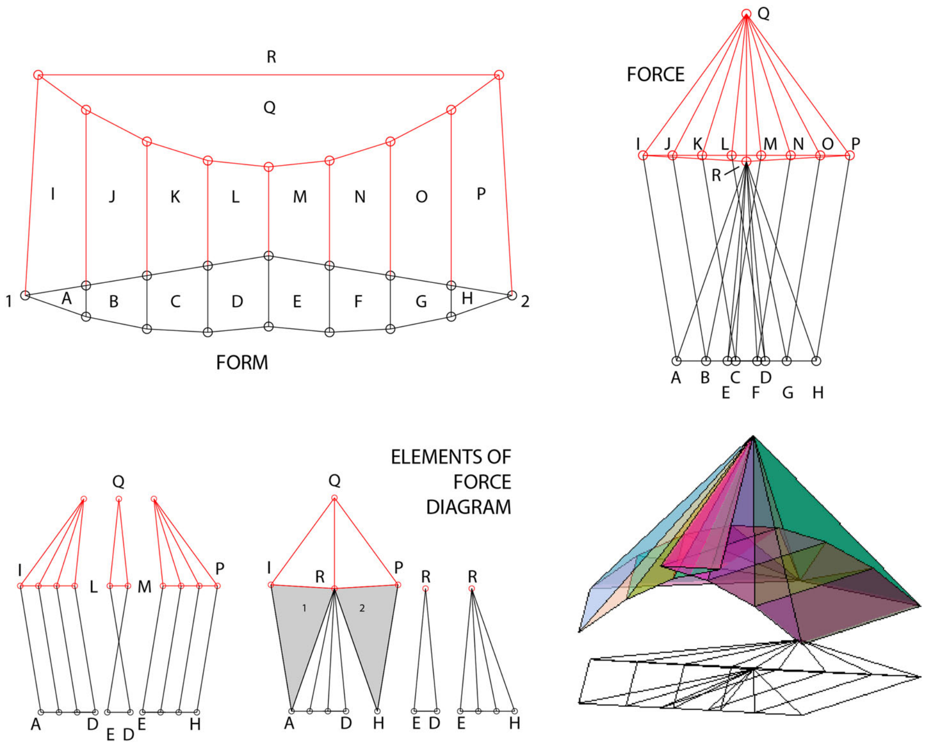

Fig. 5: Form and force reciprocal diagrams, including a funicular to apply roof loads. Lower right is the Airy stress function over the force diagram the normals of which define the form diagram

Incremental Airy Stress Functions over the Force Diagram

Airy 1:	[J, B]	=	[1,1]
Airy 2:	[K, C]	=	[1,1]
Airy 3:	[L, M, E, D]	=	[1,1,1,1]
Airy 4:	[N, F]	=	[1,1]
Airy 5:	[O, G]	=	[1,1]
Airy 6:	[Q]	=	[1]

(all other nodal values zero)

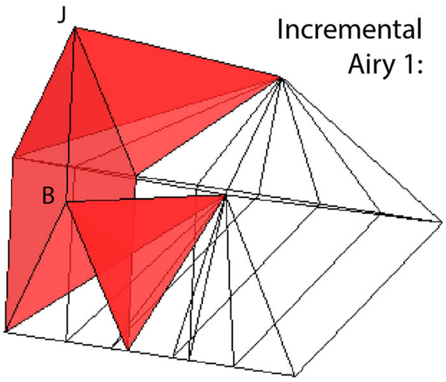

Fig. 6: One of the incremental Airy stress functions over the force diagram that will be used to generate the mechanisms

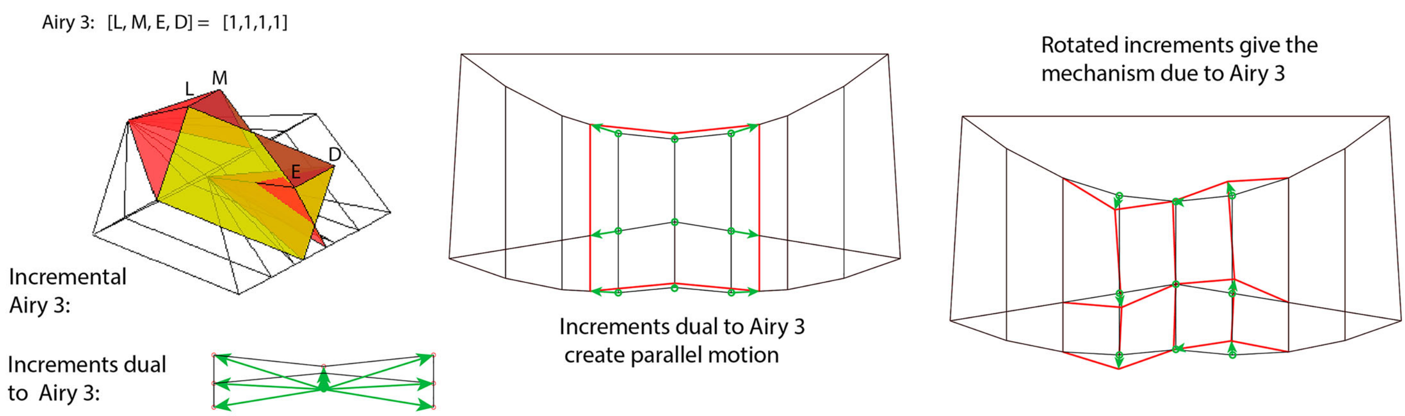

Fig. 7: Using an incremental Airy stress function over the force diagram to generate a mechanism in the form diagram. Here, the incremental stress function Airy 3 raises the crossed quad LMED by unit height, with all other nodes remaining zero. All faces remain planar, and normals to these faces define the nodal increments (lower left). These are added to the form diagram (centre) and then rotated by 90° to obtain the mechanism (right)

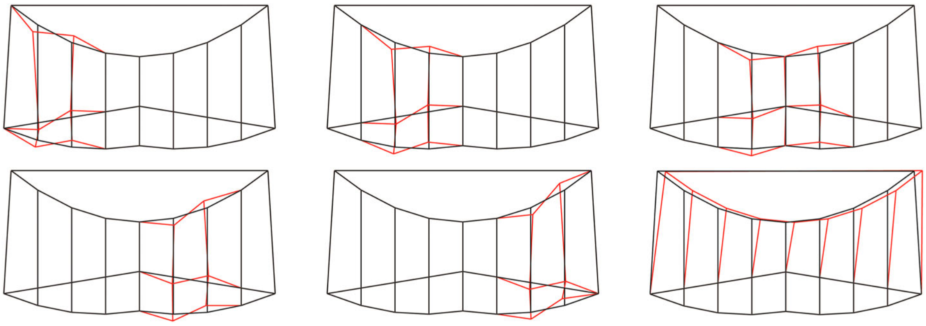

Fig. 8: The six independent mechanisms for the central section generated by the rotated incremental Airy approach. The sixth mechanism, involving only the external funicular, is irrelevant

stresses in order to determine the stability. For each mechanism, the corresponding bar rotations are readily determined. The total potential energy associated with that mechanism is then the weighted sum of the rectangular areas *TL* of the Maxwell–Minkowski diagram. The bar lengths *L* and tensions *T* are determined from the original graphic statics, and the weights are the squares of the bar rotations. The external funicular members are not included in this summation, as the effects of the external loads on the stability are included within Eq. (1). *Figure 9* gives an example calculation, using the mechanism associated with the incremental Airy 3.

This choice of geometry is given by the angles listed in *Fig. 4*. It is close to the actual geometry of the Chiasso roof. Since all five basis mechanisms of the structure are found to be unstable under the action of symmetric roof loads, it may be concluded that, were Chiasso to be a pin-jointed truss, it would be unstable.

Further analysis reveals that the stability of such a truss depends heavily upon the end reactions. These are not in general vertical, as was assumed initially, but depend quite sensitively upon the truss geometry. These reactions may be inclined inwards or outwards.[27] The stability results above were for the choice of angles in *Fig. 4*, and the requirement for equilibrium leads to the comparatively deep truss

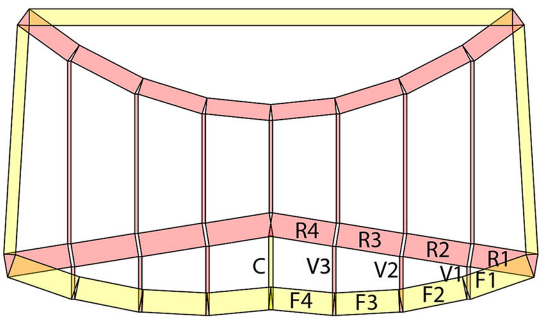

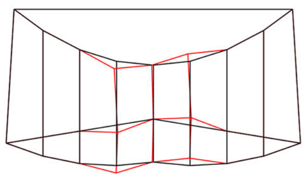

Airy 3 mechanism

$$k = \sum TL\theta^2 = -0.2330$$

therefore unstable

	L	T	θ²	LTθ²
R1	1.0132	-7.0559	0	0
R2	1.0132	-7.0559	0	0
R3	1.0132	-7.0559	0.1582	-1.1311
R4	1.0132	-7.0559	0.1582	-1.1311
F1	1.0595	7.1587	0	0
F2	1.0202	6.8932	0	0
F3	1.0015	6.7666	0.1582	1.0722
F4	1.0044	6.7865	0.1582	1.0785
V1	0.5130	-1.0000	0	0
V2	0.8780	-1.0000	0	0
V3	1.0950	-1.0000	0.0062	-0.0068
C	1.1640	1.2703	0.0026	0.0038

Fig. 9: The weighted areas of the Maxwell–Minkowski sum show that the mechanism associated with the incremental stress function Airy 3 is unstable

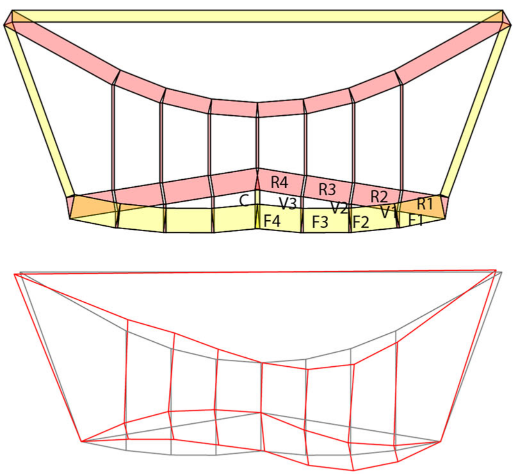

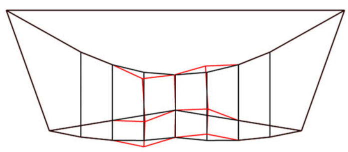

Airy 3 mechanism

$$k = \sum TL\theta^2$$

$$= +0.6752$$

therefore stable

	L	T	θ²	LTθ²
R1	1.0132	-9.0702	0	0
R2	1.0132	-9.0702	0	0
R3	1.0132	-9.0702	0.1612	-1.4814
R4	1.0132	-9.0702	0.1612	-1.4814
F1	1.0198	10.4062	0	0
F2	1.0052	10.2570	0	0
F3	1.0000	10.2042	0.1612	1.6449
F4	1.0044	10.2491	0.1612	1.6594
V1	0.3630	-1.0000	0	0
V2	0.6280	-1.0000	0	0
V3	0.7950	-1.0000	0.0071	-0.0057
C	0.8640	1.9184	0.0021	0.0034

Fig. 10: The Maxwell–Minkowski diagram for a roof truss of different geometry, loaded from above. Equilibrium requires the end reactions to be outwardly-directed. These create additional tensions across the structure, and all the mechanisms are thereby stabilised. The eigenmode, lower left, is the least stable, but it is stable. The stability summation for the basis mechanism Airy3 is given at the right

of *Fig. 9*, which has inward-pointing reactions. These reactions are associated with increased compressions across the structure, all of the modes of which have been found to be unstable.

However, a small change to the structural geometry, changing the eaves angle β to 0.2, leads to the configuration shown in Fig. 10. For this slimmer geometry to be in equilibrium with the symmetrical loads, the reactions must incline outwards, with consequent additional horizontal tensions across the whole structure, which have a stabilising effect. Analysis reveals each of the basis mechanisms to be stable under the action of symmetric roof loads applied from above. However, it is necessary to check that there is no linear combination of mechanisms that is unstable. To this end, the calculated bar lengths and tensions may be combined with the bar rotations and nodal displacements to determine the stiffness and constraint matrices **K** and **B** and solve the generalised eigenvalue problem, Eq. (4).

Perhaps surprisingly, all mechanisms of this slimmer roof are stable with its outward-leaning reactions, even with the loading applied from above. The least stable mode—which is stable nevertheless—is illustrated in Fig. 10 and involves a long-wavelength deformation resembling the deformation associated with overall asymmetric loading.

It is instructive to compare the stability summations of the Airy 3 mechanism in *Figs. 9, 10* for the deeper and slimmer trusses, respectively. The Airy 3 mechanism is a basis mechanism of no particular significance, but the insights to be obtained here will apply more generally. The first point to note in the stability tables is that the contributions to the summations from the vertical members are almost negligible in comparison to those from the main upper and lower chord members. The upper and lower chord members each have a length around L, and the members that move all have the same rotation angle. The stability is thus largely determined by the relative dominance of the tensions and compressions. For the deeper truss, the roof compressions are around −7.05 and their contributions dominate over the lower members, whose tensions average +6.9. For the slimmer truss, the roof compressions are higher at −9.07, but the tensions below are higher yet at +10.2. The tension contributions thus dominate and, for this mode of deformation, the slimmer truss is thus stabilised by the forces. This is even noticeable visually, from the dominance of the yellow over the pink in the Maxwell–Minkowski diagram of Fig. 10. Such considerations apply more generally—the outward-pointing end reactions bias

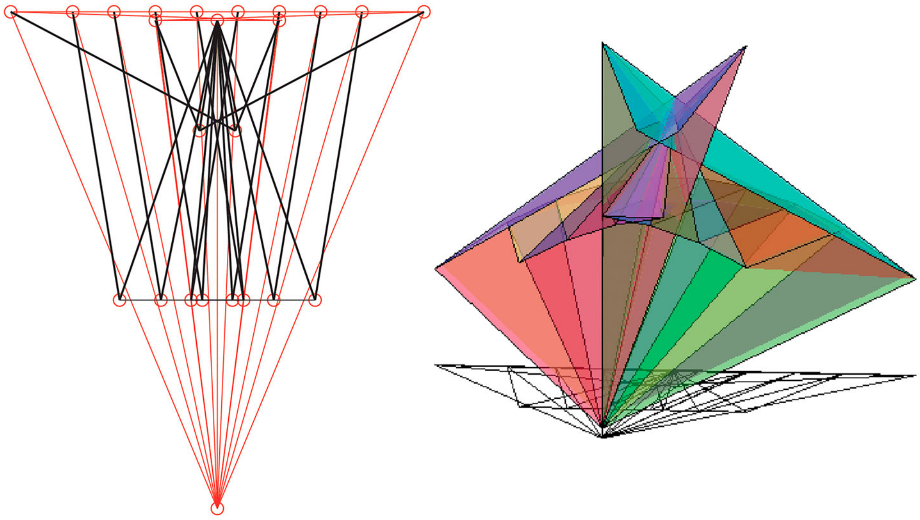

Fig. 11: The force diagram for the full truss, and the dual Airy stress function that generates the form diagram

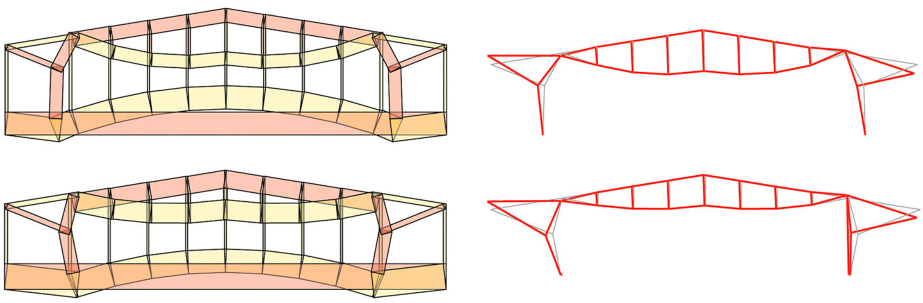

Fig. 12: Maxwell–Minkowski diagrams for the full truss. An external funicular below each truss applies the loads to the roof surface but its members are not included in the stability summations. For the sake of this example, the column feet are assumed to be pinned. For the deeper truss (top), all eigen-mechanisms are unstable, and the most unstable is shown (upper right). For the slimmer truss, the columns tilt outwards. The mechanisms associated with the central quads are stabilised by the resulting tension across the centre, but the mechanism (lower right) involving rotations of the columns is unstable

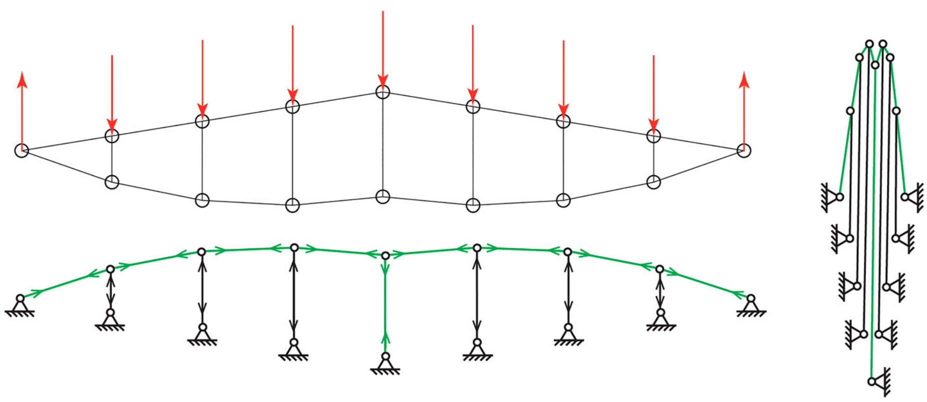

Fig. 13: The out-of-plane stability is perhaps best visualised by inverting the roof, and then looking along the truss, thereby reducing the problem to one of an “equivalent clothes line”

the stability summations in favour of the tensions, and all mechanisms are stabilised.

In summary, if the central section of the Chiasso shed were a pin-jointed truss it would be unstable against in-plane deformations when loaded from above. For this specific load case, small changes to the truss geometry can lead to in-plane stability of these localised mechanisms. However, the stability of the wider structure must be examined.

The Full Truss

The analysis is now expanded to include the outer bays and supporting columns. Again, an external funicular is added in order to apply the roof loads, although on this occasion it has been found more convenient to locate the funicular below the structure. The only boundary conditions are that the two column feet are assumed to be perfectly pinned whilst being restrained against any translation. This is clearly somewhat artificial, as the columns and foundations at Chiasso are stocky, with considerable flexural rigidity. The force diagram is shown in Fig. 11. The locations of the "pinned" columns are dictated by equilibrium, and the deeper roof truss, which is close to the Chiasso geometry, has support columns the tops of which lean inwards.

The resulting form diagram has $v = 33$ vertices and $e = 55$ edges with $r = 4$ reaction components at the pinned supports. The Calladine count gives $2v - e - r = 2(33) - 55 - 4 = 7 = m - s$. There being only the $s = 1$ state of self-stress associated with the loading, there are thus $m = 8$ independent mechanisms. Five of these may be taken as those of the central section used earlier. Three other mechanisms may be found using the incremental Airy approach, adopting local stress functions over the force diagram that respect the no-displacement boundary conditions at the pinned feet. After calculating bar rotations and then solving the generalised eigenvalue problem, it is found that all mechanisms for this geometry are unstable. For the most unstable mechanism (Fig. 12) the central section stays comparatively rigid but the column regions flex. The full analysis is then repeated for the slimmer roof truss with the smaller eaves angle.

For the slimmer roof truss, equilibrium dictates that the columns lean outwards, and as was the case earlier for the centre span alone, this leads to an overall increase in tension across the centre that stabilises the four-bar linkages in the central bays. However, this increase in tension does not stabilise the sway modes of the overall roof.

The deeper truss is close to the geometry of the actual Chiasso structure, and it is again concluded that, were it a pin-jointed truss, then it would be unstable under uniform symmetric loads. The slimmer truss with smaller eaves angles is also unstable for this load case. This is all unsurprising, as the hypothetical structure resembles a portal frame with pinned joints. In reality, the columns are stocky with significant bending capacity, and one end of the roof is attached to the adjacent building such that stability against sway is provided by membrane action within the roof plane.

Numerous geometric variants were explored to see if it was possible to create a roof of similar geometry that was stable even with all column joints assumed to be pins. These attempts were unsuccessful. Geometries where the columns inclined even more markedly outwards increased the central tensions, and although this further stabilised the inner quads they were unable to provide tension stiffening to the column regions. This was true even if the outer bays were flipped above the roof, creating trusses that more closely resembled the global bending moment diagram. Applying the roof loads at the nodes of the lower chord rather than on the roof also made little difference to the overall stability, given the small contributions of the vertical hangers to the energy summation.

Out-of-Plane Stability

The roof truss is not pin-jointed, and its existence demonstrates that it is stable. An explanation for how it can sustain asymmetric loads has been put forward earlier[2,3,12] in that the rafter and adjacent roof can act in the same manner as the stiff beam of one of Maillart's deck-stiffened bridges. However, one may also consider the out-of-plane stability of the trusses. It is chosen to approximate the roof nodes as pinned supports that are prevented from translating horizontally by the overall membrane action of the roof, and to consider the out-of-plane stability of the lower tension chord below the effectively rigid roof (Fig. 13).

This is most readily accomplished by noting that the $TL\theta^2$ term of the energy summation may be written $(T/L)w^2$, where w is the lateral displacement of one end of the bar relative to the other end. Looking along the truss projects all objects onto a vertical plane. The vertical length and force components of a bar inclined at an angle β to the horizontal are $L \sin\beta$ and $T \sin\beta$, thus the ratio $(T \sin\beta)/(L \sin\beta) = T/L$ is unchanged by the projection. The out-of-plane stability may therefore be determined by considering a one-dimensional truss, with all members co-linear. The system resembles seven pendula (albeit that most of the pendula here are in compression). These are co-linear but separately supported, with their free ends connected by vertical tensioning wires. There are seven mechanisms, one per pendulum. The total potential energy is readily evaluated using Eq. (1), giving a quadratic form in the tip displacements $\mathbf{w}$. The eigenvalues reveal that all out-of-plane modes are stabilised by the state of self-stress.

Turning the central form diagram upside down shows that the system is a more complicated variant of the more familiar clothes prop problem. A clothes prop is stable if its base lies below the end-supports of the washing line. Here, there are seven clothes props. The central one is actually in tension and—in the upside-down perspective—all bases are below the line joining the end supports. The out-of-plane stability is thus perhaps unsurprising.

The Chiasso shed possesses a number of additional longitudinal members that connect between adjacent trusses. These members, and the truss members themselves, are comparatively thick with rigid connections. However, even if these lower members were pin-jointed, the above analysis reveals that the trusses would be stable against out-of-plane movement.

Conclusions

The new method of graphic stability has been demonstrated using the roof trusses at Maillart's Chiasso shed as an example. According to this approach, were the trusses to be perfectly pin-jointed, they would be unstable under uniform roof loads. A variant design with a shallower truss was found to provide tensions from its supports and thereby exhibit greater stability, despite the number of quadrilaterals in its form. However, this still lacked stability against overall sway. The geometry of the lower tension chord members at Chiasso was found to provide stability against out-of-plane movement, although as Maillart lacked the tools to demonstrate this, he ensured stability by providing additional perpendicular girders.

Having stood for almost a century, the Chiasso roof is clearly stable. It gains its stability from the combined action of roof and lower chord in a manner akin to that found in Maillart's deck-stiffened bridges from around the same time. Despite the success of Chiasso, designers should nevertheless be wary of simply copying Maillart. Stability is subtle, equilibrium is not enough and excessive optimisation for equilibrium is potentially dangerous. Graphic statics has the potential to lead to efficient but unstable designs. The new methods of graphical stability developed by Millar et al.[1]—illustrated in this paper—may be a significant advance in this regard.

Disclosure Statement

No potential conflict of interest was reported by the authors.

References

[1] Millar C, McRobie A, Baker W. A graphical method for determining truss stability. Proc IASS Symp 2020 & 7th Int. Conf. on Spatial Structures, 2020, Guilford, UK. (Behnejad SA, Parke GAR and Samavati OA, eds.), 2020.

[2] Zastavni D. *La Conception Chez Robert Maillart: Morphogenèse des Structures Architecturales*, 339–351. Louvain-la-Neuve: Unité d'Architecture, Université Catholique de Louvain, 2007.

[3] Zastavni D. The structural design of Maillart's Chiasso Shed (1924): A graphic procedure. *Struct Eng Int*. 2008; 18(3): 247–252. doi:10.2749/101686608785096496.

[4] Stevin S. *De Weeghdaet Praxis artis ponderariae*. Leyden: Druckerye C. Plantij, 1586.

[5] Varignon P. *Projet d'une Nouvelle Méchanique*. Paris: Chez Martin & Boudot, 1687.

[6] Maxwell JC. On reciprocal figures and diagram of forces. *Philos Mag*. 1864; 26: 250–261. doi:10.1017/S0080456800026351.

[7] Maxwell JC. On reciprocal figures, frames and diagram of forces. *Trans Royal Soc Edinburgh*. 1870; 26: 1–40. doi:10.1017/s0080456800026351.

[8] Cremona L. *Graphical Statics. Two Treatises on the Graphical Calculus and Reciprocal Figures in Graphical Statics*. Oxford: Clarendon Press, 1890. (Transl. Thomas Hudson Beare.) 1890.

[9] Culmann K. *Die Graphische Statik*. Zürich: Meyer und Zeller, 1866.

[10] Beghini LL, Carrion J, Beghini A, Mazurek A, Baker WF. Structural optimization using graphic statics. *Struct Multidisc Optim*. 2013; 49 (3): 351–366. doi:10.1007/s00158-0133-1002-x.

[11] Guest SD. The stiffness of prestressed frameworks: A unifying approach. *Int J Solids Struct*. 2006; 43: 3–4, 842–854.

[12] Billington D. *Robert Maillart, Builder, Designer, and Artist*. Cambridge UK; New York: Cambridge University Press, 1997.

[13] Adão da Fonseca A, Millanes Mato F. Infant Henrique bridge over the River Douro, Porto. *Struct Eng Int*. 2005; 15(2): 5–87.

[14] Bill M. *Robert Maillart, Bridges and Constructions*. Erlenbach-Zürich: Verlag für Architektur, 1949.

[15] Billington D. Deck-stiffened arch bridges of Robert Maillart. *J Struct Div, ASCE*. 1973; 99(7): 1527–1539.

[16] Verswijver K, De Meyer R, Denys R, De Kooning E. The writings of Belgian Engineer Arthur Vierendeel (1852-1940): homo universalis or contemporary propagandist? Proc 3rd Int Cong on Construction History, Cottbus, May 2009.

[17] Lambin A, Christophe P. Le pont Vierendeel. Rapport sur les essais jusqu'à la rupture effectués, au parc de Tervuren, par M. Vierendeel, sur un pont métallique de 31m.50 de portée, avec des poutres à arcades de son système. *Annales des travaux publics de Belgique*. 1898; 55(1): 53–139.

[18] Pons-Poblet JM. The Vierendeel truss: past and present of an innovative typology. *Arquitetura Revista*. 2019; 15(1): 193–211.

[19] Wolfe WS. *Graphical Analysis – A Text Book in Graphic Statics*. New York: McGraw-Hill, 1921.

[20] Allen E, Zalewski W. *Form and Forces: Designing Efficient Expressive Structures*. Chichester: Wiley, 2009.

[21] Mitchell T, Baker W, McRobie A, Mazurek A. Mechanisms and states of self-stress of planar trusses using graphic statics, part I: The fundamental theorem of linear algebra and the Airy stress function. *Int J Space Struct*. 2016; 31: 102–111. doi:10.1177/0266351116660791.

[22] McRobie A, Baker W, Mitchell T, Konstantatou M. Mechanisms and states of self-stress of planar trusses using graphic statics, part II: applications and extensions. *Int J Space Struct*. 2016; 31: 102–111. doi:10.1177/0266351116660791.

[23] Zanni G, Pennock GR. A unified graphical approach to the static analysis of axially loaded structures. *Mech Mach Theory*. 2009; 44: 2187–2203. doi:10.1016/j.mechmachtheory.2009.07.002.

[24] McRobie A. Maxwell and Rankine reciprocal diagrams via Minkowski sums for 2D and 3D trusses under load. *Int J Space Struct*. 2016; 31: 203–216. doi:10.1177/0266351116660800.

[25] Crapo H, Whiteley W. Spaces of stresses, projections and parallel drawings for spherical polyhedra. *Beitr Algebr Geom*. 1994; 35(2): 259–281.

[26] McRobie A, Millar C, Baker WF. Stability of trusses by graphic statics. *R Soc Open Sci*. 2021; 8: 18. doi:10.1098/rsos.2019702016.

[27] Ciblac T. Structure Computation Tools in Architectural Design, *Architecture in Computro* [26th eCAADe Conference Proceedings / ISBN 978-0-9541183-7-2] Antwerpen (Belgium) 17-20 September 2008, pp. 275-282 http://papers.cumincad.org/cgi-bin/works/Show?ecaade2008_023, 2008.

[28] Calladine CR. Buckminster Fuller's "tensegrity" structures and Clerk Maxwell's rules for the construction of stiff frames. *Int J Solids Struct*. 1978; 14: 161–172.